

Electronic spectroscopy and ionization potentials for YbOH and YbOCH₃Thomas D. Persinger¹, Jiande Han,¹ Anh T. Le,² Timothy C. Steimle,³ and Michael C. Heaven^{1,*}¹*Department of Chemistry, Emory University, Atlanta, Georgia 30322, USA*²*School of Chemistry and Biochemistry, Georgia Institute of Technology, Atlanta, Georgia 30318, USA*³*School of Molecular Sciences, Arizona State University, Tempe, Arizona 85287, USA* (Received 28 December 2022; revised 5 February 2023; accepted 21 February 2023; published 10 March 2023)

The polyatomic molecules YbOH and YbOCH₃ have been recognized as being of potential value for spectroscopic experiments that explore charge-parity and time-reversal symmetry violation effects. These measurements require very high precision, which, in turn, will necessitate that the molecules be manipulated at ultracold temperatures. Both YbOH and YbOCH₃ have electronic transitions that appear suitable for laser cooling ($\tilde{A}^2\Pi_{1/2}-\tilde{X}^2\Sigma^+$ and $\tilde{A}^2E_{1/2}-\tilde{X}^2A_1$, respectively) but the currently available spectroscopic data are not sufficient to determine the extent to which population leaks may compromise the optical cooling processes. A further complication is that the quantum states of interest for these measurements will need to be selectively populated. The $\tilde{A}-\tilde{X}$ band systems of both YbOH and YbOCH₃ show evidence of vibronic perturbations, such that there are unassigned vibronic features at energies that are just above the origin bands. In the present study we have recorded spectra for the $\tilde{A}^2\Pi_{1/2}-\tilde{X}^2\Sigma^+$ transition of jet-cooled YbOD to facilitate the vibronic assignments. In addition, spectra for the $\tilde{B}^2\Sigma^+-\tilde{X}^2\Sigma^+$ transition of YbOH were recorded, establishing the origin band at 20 473.8 cm⁻¹. Previously, the reaction of Yb with CH₃OH has been used to generate gas-phase YbOCH₃. As this reaction also yields YbOH, there have been complications in spectroscopic studies of YbOCH₃ due to overlap of the $\tilde{A}-\tilde{X}$ band systems. To identify specific regions of overlap, resonantly enhanced two-photon ionization spectra were recorded using mass-resolved detection of the YbOH⁺ and YbOCH₃⁺ ions. These data confirmed the overlap of vibronic bands near 17 640 and 17 680 cm⁻¹. Two-photon ionization spectroscopy also provided accurate ionization energies (IE), IE(YbOH) = 45 788(10) and IE(YbOCH₃) = 45 283(10) cm⁻¹. The IE for YbOH is relevant to problems encountered in previous attempts to determine the bond-dissociation energy of YbOH⁺.

DOI: [10.1103/PhysRevA.107.032810](https://doi.org/10.1103/PhysRevA.107.032810)**I. INTRODUCTION**

A subset of small molecules that contain the element Yb have been identified as being promising candidates for studies of parity- and time-violating phenomena that are beyond the predictions of the Standard Model. The precision measurements needed to investigate these properties, such as the electron electric-dipole moment (eEDM), would benefit from having ultracold molecular samples. One approach to achieving the necessary conditions is to apply laser-cooling techniques. Ionic molecules that include Yb in the +1 oxidation state show promise for laser cooling, and significant cooling has been demonstrated for YbF [1,2] and YbOH [3]. Noteworthy is the recent demonstration of laser cooling and subsequent magneto-optical trapping of the molecule CaOH [4], which has many similarities to YbOH.

Another desirable property for studies of parity-violating effects in heavy molecules is that they usually possess closely spaced parity doublets [5,6]. Molecules in such parity doublets can be fully polarized in the laboratory frame and hence the large internal effective electric fields utilized. For a linear molecule, such as YbOH, excitation of one quantum of the

bending vibrational mode results in closely spaced pairs of energy levels associated with $l = +1$ and -1 , where l is the projection of the vibrational angular momentum along the internuclear axis [4–6]. Nonlinear symmetric-top molecules have even closer \pm parity splittings associated with rotation about the high-order symmetry axis (a or c). Hence, the $K_a = \pm 1$ rotational levels of YbOCH₃ are of interest (where K_a is the projection of the rotational angular momentum along the molecular a axis) [4,5,7,8].

Recent spectroscopic studies of YbOH [9–11] and YbOCH₃ [7] have been carried out in part to evaluate the full potential for laser cooling and transitions that might be used to populate the levels of interest. Laser-cooling schemes have been devised for the $\tilde{A}^2\Pi_{1/2}-\tilde{X}^2\Sigma^+$ (YbOH) [3] and $\tilde{A}^2E_{1/2}-\tilde{X}^2A_1$ (YbOCH₃) [7] transitions. Because these transitions are predominantly the Yb⁺6s → 6p electron promotion, where both orbitals are nonbonding, the Franck-Condon factor distributions strongly favor $\Delta v = 0$ vibronic bands. This condition is needed to confine the state populations to the upper and lower levels of the cooling transition. However, radiative leakage to other electronic states is a potential complication for Yb⁺X⁻ species [7,10,12]. The low-energy electronic states of concern are derived from the Yb⁺(4f¹³ 6s²)X⁻ configuration. In the example of YbF, vibronic transitions that occur in the same spectral region as

*Corresponding author: mheaven@emory.edu

the $A^2\Pi_{1/2}-\tilde{X}^2\Sigma^+$ bands have been assigned to upper states that arise from the $4f^{13}(^2F_{5/2})6s^2$ configuration. Zhang *et al.* [12] analyzed perturbations between the $A^2\Pi_{1/2}$ state and the $4f^{13}(^2F_{5/2})6s^2\Omega = 1/2$ state (where Ω is the unsigned projection of the electronic angular momentum along the internuclear axis). They found that these interactions enable weak, but not negligible, radiative transitions from $A^2\Pi_{1/2}$, $v = 0$ down to the $4f^{13}(^2F_{7/2})6s^2\Omega = 1/2$ state. The theoretical calculations used in making this prediction were recently validated through direct observation of the $4f^{13}(^2F_{7/2})6s^2$ states [13].

Visible excitation spectra in the region of the $\tilde{A}^2\Pi_{1/2}-\tilde{X}^2\Sigma^+$ transition of YbOH have also revealed additional vibronic features that have been tentatively attributed to states arising from the $\text{Yb}^+(4f^{13}(^2F_{5/2})6s^2)\text{OH}^-$ configuration. Mengesha *et al.* [10] used a combination of laser-induced fluorescence (LIF) and dispersed laser-induced fluorescence (DLIF) measurements of a supersonic jet-cooled sample to investigate vibronic-state assignments and branching ratios for radiative relaxation. Spectra taken over the range 17 300–17 950 cm^{-1} included 11 bands that were assigned to 9 vibronically excited states. A band at 17 643 cm^{-1} was of particular interest as it had a dominant emission down to the ground-state level with one quantum of the bending vibration excited. Clearly, this could be used to populate the highly polarizable parity doublets desired for precision measurements. The upper states of several of these 11 vibronic bands (including the 17 643 cm^{-1} band) could not be unambiguously assigned. In the present work we have examined the excitation spectrum of YbOD in the 17 300–17 950 cm^{-1} range, in hopes that the isotope shift data will facilitate the vibronic-state assignment process.

Emission from the YbOH $\tilde{A}^2\Pi_{1/2}$ state to the $4f^{13}(^2F_{7/2})6s^2$ states, expected to be weak given that it is nominally a $6s \rightarrow 4f$ transition, was not observed by Mengesha *et al.* [10]. In addition to being weak, it is probable that this emission occurs at wavelengths that were too long for their detection system. Emission from the $\tilde{B}^2\Sigma^+$ state to the $4f^{13}(^2F_{7/2})6s^2$ states is predicted to fall in a more convenient spectral region, but no experimental data for the $\tilde{B}-\tilde{X}$ system have been published.

Direct $\tilde{B}^2\Sigma^+(0, 0^0, 0)-\tilde{X}^2\Sigma^+(0, 0^0, 0)$ excitation of YbOH is relevant to laser-cooling and optical-detection schemes in a manner analogous to the role that the $\tilde{B}^2\Sigma^+(0, 0^0, 0)$ state plays in the recently demonstrated magneto-optical trapping and sub-Doppler cooling of CaOH [4]. Furthermore, characterization of the $\tilde{B}^2\Sigma^+$ state can validate recent theoretical predictions used to quantify the observed branching ratios relevant to laser cooling of YbOH [11,14]. In that study, it was shown that coupling between the $\tilde{A}^2\Pi$ and $\tilde{B}^2\Sigma^+$ states mixes some bending motion into the wave function for the $\tilde{A}^2\Pi(0, 0^0, 0)$ level, and thus allows the nominally symmetry forbidden $\tilde{A}^2\Pi_{1/2}(0, 0^0, 0)-\tilde{X}^2\Sigma^+(0, 1^1, 0)$ transition to have significant strength. The theoretical prediction [11,14] places the $\tilde{B}^2\Sigma^+(0, 0^0, 0)$ vibronic level 2935 cm^{-1} above the $\tilde{A}^2\Pi_{1/2}(0, 0^0, 0)$ level and predicts a characteristic stretching Yb-OH vibrational spacing of 559 cm^{-1} . Experimental data on the $\tilde{B}^2\Sigma^+$ state are sought, in part, to gauge the reliability

of these theoretical predictions. Here we report LIF and DLIF spectra for the $\tilde{B}^2\Sigma^+-\tilde{X}^2\Sigma^+$ transition.

Resonantly enhanced two-photon ionization (RE2PI) spectra, with mass-resolved YbOH/D⁺ ion detection, were examined to confirm the molecular carriers for the bands attributed to YbOH/D. The setup used for these measurements also provided a facile means for determination of the ionization energy (IE) [15]. The value obtained for YbOH was 45 788(10) cm^{-1} . This result is useful for the interpretation of experiments that yielded contradictory results for the bond-dissociation energies of YbOH and YbOH⁺ [16–18] (*infravide*).

A preliminary study of the $\tilde{A}^2E-\tilde{X}^2A_1$ band system of YbOCH₃/YbOCD₃ using LIF detection was reported by Augenbraun *et al.* [7] As expected, the characteristics of this transition were found to be closely similar to those of the corresponding transitions of YbF and YbOH. The LIF spectra in that study were heavily overlapped because the technique used to generate gas-phase YbOCH₃ molecules (i.e., reaction of laser-ablated Yb with CH₃OH) also produces YbOH. The present study of YbOCH₃ was restricted to the matter of confirming the molecular carrier of previously observed bands in the LIF spectrum. The mass-selected RE2PI spectra were used to identify overlapping bands of the two molecules. In addition, the IE of YbOCH₃ was determined and found to be just 506 cm^{-1} below that of YbOH.

II. EXPERIMENT

The instrumentation used to record gas-phase spectra for YbOH and YbOCH₃ has been described previously [15]. Following the work of Steimle and co-workers [7,9,10], both molecules were obtained by reacting laser-ablated Yb vapor with CH₃OH (or CD₃OD for a study of YbOD). The Yb vapor was obtained by pulsed 1064-nm Nd/yttrium aluminum garnet laser ablation of the surface of a Yb rod. The rod was mounted in a Smalley-type jet expansion source [19] where it was rotated and translated to avoid pitting. CH₃OH vapor was seeded into the He carrier gas by passing the gas flow over the surface of the liquid at room temperature. This mixture was supplied to the ablation source by a pulsed valve (Parker-Hannifin series 9) at a backing pressure of 5 atm. LIF and DLIF spectra were recorded with the excitation laser beam set to cross the jet expansion approximately 7.5 cm downstream from the nozzle orifice. LIF was collected along an axis that was perpendicular to both the laser-beam axis and the free-jet expansion axis. For the recording of LIF data, a long-pass filter was used to reduce the scattered laser light, and the filtered fluorescence was detected by a photomultiplier tube (Photonis XP2020). DLIF spectra were obtained when the long-pass filter was replaced by a 0.25-m monochromator (Jarrell-Ash 82–410).

Two tunable pulsed dye-laser systems were used in these experiments. The dye lasers operated with linewidths (full width at half maximum) of approximately 0.3 cm^{-1} . Wavelength calibration of the dye lasers was established using a Bristol Instruments model 821 wavemeter. Fluorescence decay curves were acquired using a digital oscilloscope (LeCroy WaveSurfer 24Xs) to signal average 256 laser pulses per trace.

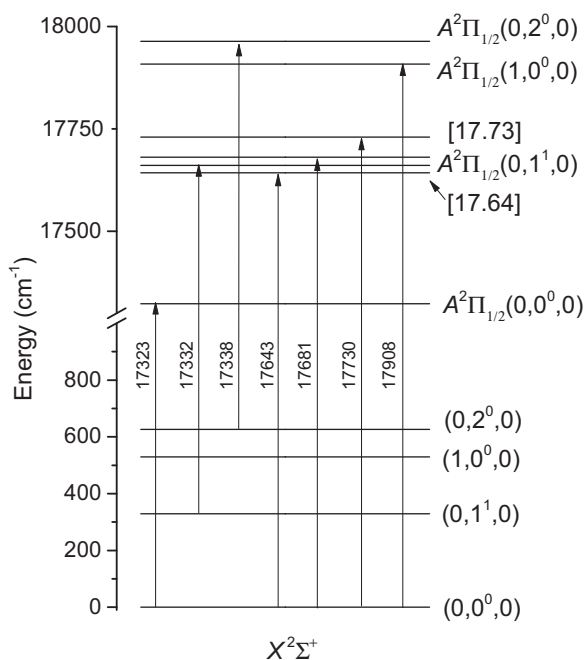


FIG. 1. Energy-level diagram for the YbOH transitions examined in the present study. The level immediately above $\tilde{A}^2\Pi_{1/2}(0,1^1,0)$ is [17.68]. This label was omitted due to space limitations. The two levels observed for the $\tilde{B}^2\Sigma^+$ state, $(0,0^0,0)$ and $(1,0^0,0)$, are off scale at 20 473 and 21 033 cm^{-1} , respectively.

RE2PI and photoionization efficiency (PIE) measurements were carried out in a differentially pumped vacuum chamber that was equipped for time-of-flight mass spectrometry and photoelectron detection [15]. RE2PI and PIE spectra were recorded with mass-resolved cation detection. RE2PI data for transitions occurring in the near-UV spectral range were obtained using one-color, two-photon ionization. All two-color measurements were carried out using spatially overlapped, counterpropagating laser beams.

PIE curves were recorded with the first laser set to populate an excited state of YbOH or YbOCH₃. The wavelength of the second laser was then swept to locate the onset of ionization. These measurements were conducted with the ionization zone located between the charged electrodes of the mass spectrometer. The local electric field of 364 V cm^{-1} caused a depression of the IE by 115 cm^{-1} (this value is based on previous measurements where the field-free IE determined by pulsed field ionization - zero kinetic energy (PFI-ZEKE) photoelectron spectroscopy was compared to the IE obtained in the PIE measurements. For example, see Ref. [20]).

III. RESULTS AND ANALYSIS

A. Effect of isotopic substitution on the $\tilde{A}^2\Pi_{1/2}-\tilde{X}^2\Sigma^+$ transition of YbOH/D

In the following we label the vibrational levels of YbOH/D using the notation $(v_1, v_2^{|l|}, v_3)$ where v_1 is the vibrational quantum number for the Yb-OH stretch, v_2 is the bend, $|l|$ is the unsigned projection of the vibrational angular momentum along the cylinder axis, and v_3 is the O-H stretch (not active in the spectra reported here). Figure 1 shows an energy-level

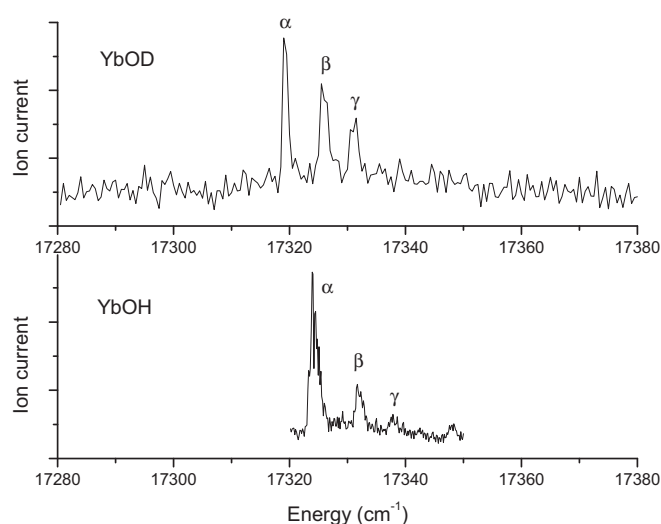


FIG. 2. RE2PI scan of the $A^2\Pi_{1/2}-X^2\Sigma^+$ transitions of YbOH and YbOD, 17 280–17 380 cm^{-1} . Features labeled α , β , and γ are assigned as the $\tilde{A}^2\Pi_{1/2}(0,0^0,0)-\tilde{X}^2\Sigma^+(0,0^0,0)$, $\tilde{A}^2\Pi_{1/2}(0,1^1,0)-\tilde{X}^2\Sigma^+(0,1^1,0)$, and $\tilde{A}^2\Pi_{1/2}(0,2^0,0)-\tilde{X}^2\Sigma^+(0,2^0,0)$ transitions, respectively. Corresponding assignments apply to the redshifted YbOD bands.

diagram for the transitions of YbOH below 18 000 cm^{-1} that were examined in this study.

As noted in the Introduction, several bands of YbOH observed in the region of the $\tilde{A}^2\Pi_{1/2}-\tilde{X}^2\Sigma^+$ transition have yet to be assigned. Spectra for YbOD were recorded in hopes of advancing the assignment of the vibronic structure. Figures 2, 3, and 4 show vibrationally resolved RE2PI spectra for YbOH and YbOD. Figure 2 shows bands near the origin transition that occurs at 17 323 cm^{-1} for YbOH. There is a nearby band at 17 332 [10] and another, even weaker feature at 17 338 cm^{-1} (not reported previously). Relative to the origin band of YbOH, the origin of YbOD is shifted down by 5 cm^{-1} to

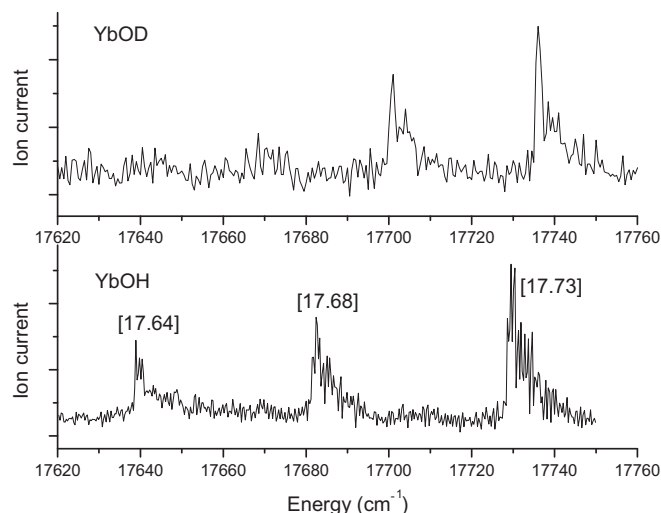


FIG. 3. RE2PI scan of the $A^2\Pi_{1/2}-X^2\Sigma^+$ transitions of YbOH and YbOD, 17 620–17 760 cm^{-1} . YbOH features are labeled according to the scheme used by Mengesha *et al.* [10]. See text for details.

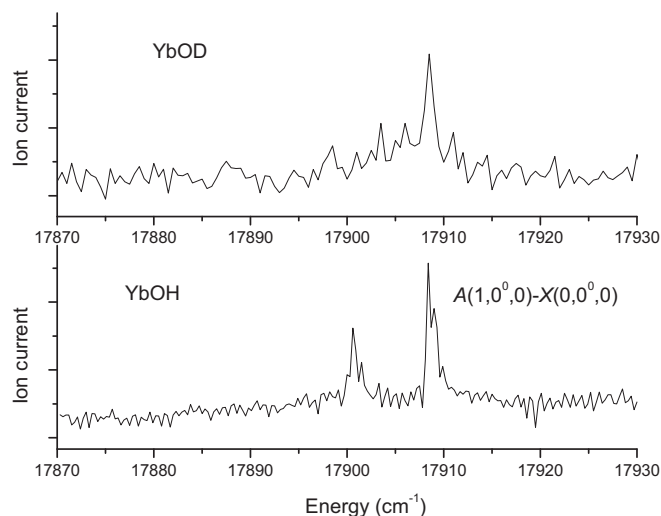


FIG. 4. RE2PI scan of the $A^2\Pi_{1/2}-X^2\Sigma^+$ transitions of YbOH and YbOD, 17 870–17 930 cm^{-1} .

17 318 cm^{-1} , and it also is accompanied by weaker features at 17 325 and 17 332 cm^{-1} . Mengesha *et al.* [10] had speculated that the YbOH band at 17 332 cm^{-1} , just 9 cm^{-1} above the origin, might indicate that the excited molecule is slightly bent, such that the 17 332 cm^{-1} band corresponds to excitation of the $K_a = \pm 1$ rotational-level manifold. However, as can be seen in Fig. 2, H/D isotopic substitution has very little effect on the spacings between the first three bands. A more substantial contraction of the intervals for YbOD would be expected if these bands involved the upper-state a -axis rotation.

An alternative choice would be to assign the YbOH band at 17 332 cm^{-1} to the $\tilde{A}(0, 1^1, 0)-\tilde{X}(0, 1^1, 0)$ sequence band. The ground-state bending level is at 329 cm^{-1} , so the blueshift for the sequence band would indicate an excited-state bending interval of 338 cm^{-1} . The slightly smaller blueshift of the corresponding YbOD sequence band (7 cm^{-1}) is then consistent with the expected isotope effect. This assignment is also compatible with the observation that the YbOH 17 323- and 17 332 cm^{-1} bands exhibit closely similar DLIF spectra (see Fig. 4 of Ref. [10]). Extending this interpretation, the band at 17 339 cm^{-1} (17 333 cm^{-1} for YbOD) may be assigned to the $\tilde{A}(0, 2^0, 0)-\tilde{X}(0, 2^0, 0)$ transition. In this context we should note that jet cooling of molecules that have been created by laser-ablation processes does not yield thermal equilibrium population distributions. Typically, the rotational levels cool to effective temperatures of 5–30 K while populations remain trapped in vibrational and electronically excited states that are more difficult to cool during the rapid expansion process. For example, in their study of jet-cooled YbOH, Mengesha *et al.* [10] recorded spectra with rotational temperatures near 20 K for bands that originated from ground-state levels with vibrational energies up to 530 cm^{-1} .

Figure 3 shows the $\tilde{A}^2\Pi_{1/2}-\tilde{X}^2\Sigma^+$ spectrum in the energy range where the band associated with excitation of one quantum of the bending mode might be observed. Three bands of YbOH were observed in the 17 620–17 760 cm^{-1} range. The proposed assignment of the bending sequence band would put the $\tilde{A}(0, 1^1, 0)-\tilde{X}(0, 0^0, 0)$ transition at 17 661

cm^{-1} , but this is symmetry forbidden in the absence of vibronic coupling (see Ref. [21] Chap. II, Sec. 2). As discussed by Mengesha *et al.* [10], the $\tilde{A}^2\Pi(0, 1^1, 0)$ state is split into four components by Renner-Teller vibronic coupling ($\mu^2\Sigma^+$, $\kappa^2\Sigma^-$, $^2\Delta_{3/2}$, and $^2\Delta_{5/2}$). Due to the large spin-orbit coupling constant ($A_{SO} \sim 1350 \text{ cm}^{-1}$), the $\kappa^2\Sigma^-$ and $^2\Delta_{3/2}$ components are at quite high energies, so the transition from the $\tilde{X}(0, 0^0, 0)$ state that occurs near 17 660 cm^{-1} would terminate on the $\mu^2\Sigma^+$ bending component. Mengesha *et al.* [10] assigned the band at 17 643 cm^{-1} to this transition. The DLIF spectrum for this band was dominated by the emission to $\tilde{X}(0, 1^1, 0)$, indicating that the upper state has a substantial contribution from the bending excitation [10]. This inference was also supported by the circumstance that we could not find a corresponding band for YbOD. Presumably, isotopic substitution had reduced the vibronic coupling that permitted the observation for YbOH. However, if the assignment of the bending sequence is correct, the 17 643 cm^{-1} band cannot be assigned as excitation to $\tilde{A}(0, 1^1, 0)$. As noted by Mengesha *et al.* [10], there are several other electronic states expected in this energy range, and the bands observed in Fig. 3 are likely associated with the $\text{Yb}^+(4f^{13} 6s^2)\text{OH}/\text{D}^-$ configuration.

Mengesha *et al.* [10] also suggested that the YbOH band at 17 680 cm^{-1} might be assigned to the $\tilde{A}^2\Pi_{1/2}(0, 1^1, 0)\mu^2\Sigma^+$ Renner-Teller component, mixed with the nearby 17 730- cm^{-1} band. The closest feature in the YbOD spectrum is at 17 701 cm^{-1} . If this is the counterpart of the YbOH 17 680- cm^{-1} band, the blueshift on deuteration (19 cm^{-1}) does not agree with significant excitation of the bending mode. In an earlier study, Melville and Coxon [22] assigned the YbOH band at 17 730 cm^{-1} as the $\tilde{A}(0, 1^1, 0)-\tilde{X}(0, 0^0, 0)$ transition. Mengesha *et al.* [10] recorded the associated DLIF spectrum and observed that a progression in the Yb-OH stretch dominated. On this basis, they tentatively assigned the upper state to the $4f^{13} 6s^2$ configuration. The nearest band of YbOD was at 17 736 cm^{-1} . If we assume that these bands share the same assignment, this yields an isotopic blueshift of 6 cm^{-1} . Again, this shift would be difficult to reconcile with the $\tilde{A}(0, 1^1, 0)$ attribution.

The YbOH band at 17 908 cm^{-1} has been attributed to the $\tilde{A}(1, 0^0, 0)-\tilde{X}(0, 0^0, 0)$ transition [10,22]. This assignment was supported by the DLIF spectrum [10]. Figure 4 shows that the corresponding transition of YbOD is at almost the same energy. As the electronic band origin of YbOD is 5 cm^{-1} below that of YbOH, the \tilde{A} -state Yb-OD stretch frequency appears to be 5 cm^{-1} higher than that of YbOH. Mengesha *et al.* [10] found that the 17 900 cm^{-1} band of YbOH yielded a DLIF spectrum that was very similar to the spectrum generated using excitation at 17 908 cm^{-1} . No assignment was recommended. Unfortunately, the YbOD counterpart was not observed as it was probably below the noise level.

B. Overlap of the $\tilde{A}-\tilde{X}$ transitions of YbOH and YbOCH_3

The reaction of Yb vapor with gas-phase CH_3OH yields both YbOH and YbOCH_3 . Augenbraun *et al.* [7] used 532 nm light for the ablation of Yb, and reported that the yield of YbOCH_3 was roughly an order of magnitude greater than that of YbOH (based on LIF detection). In the present study we used 1064-nm light for Yb ablation, combined with RE2PI

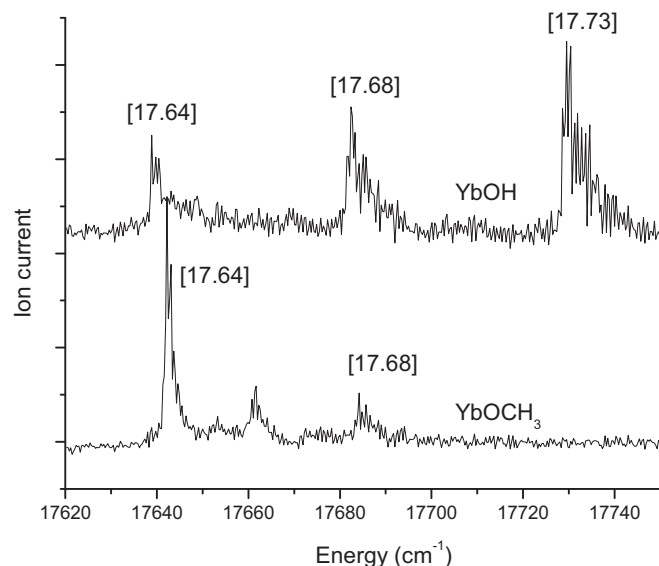


FIG. 5. RE2PI scan of the $A^2\Pi_{1/2}-X^2\Sigma^+$ transitions of YbOH and YbOCH₃, 17620–17750 cm⁻¹. YbOCH₃ features are labeled according to the scheme used by Augenbraun *et al.* [7].

detection of YbOH and YbOCH₃. The signals from these two products were approximately the same. As the $\tilde{A}-\tilde{X}$ bands of YbOH and YbOCH₃ occur in the same spectral region, we have used RE2PI measurements to identify regions where bands overlap. Figure 5 shows spectra obtained in a single sweep, with detection of the mass-resolved YbOH⁺ and YbOCH₃⁺ ions. Here, it can be seen that YbOCH₃ bands overlap the YbOH bands near 17 640 and 17 680 cm⁻¹. This is consistent with the conclusion of Augenbraun *et al.* [7] that the DLIF spectra obtained using excitation of the YbOCH₃ bands at 17 641 and 17 683 cm⁻¹ included some YbOH emission features.

C. $\tilde{B}^2\Sigma^+-\tilde{X}^2\Sigma^+$ transition of YbOH

The $\tilde{B}^2\Sigma^+-\tilde{X}^2\Sigma^+$ transition of YbOH had not been reported previously, but the transition energy could be anticipated by comparison to YbF, where the $\tilde{B}^2\Sigma^+-\tilde{X}^2\Sigma^+$ origin band was found at 21 074 cm⁻¹ [23]. The initial search for the $\tilde{B}-\tilde{X}$ system of YbOH was carried out using two-color RE2PI spectroscopy. Figure 6 shows a low-resolution spectral scan that includes the origin band at 20 473 cm⁻¹. Scanning to higher energy, the $\tilde{B}(1,0^0,0)-\tilde{X}(0,0^0,0)$ band was found at 21 033 cm⁻¹, defining an upper-state vibrational interval of $\Delta G'_{1/2} = 560(1)$ cm⁻¹. This observation also confirmed that the feature at 20 502 cm⁻¹ (Fig. 6) was the $\tilde{B}(1,0^0,0)-\tilde{X}(1,0^0,0)$ sequence band. Further confirmation that the feature at 20 743 cm⁻¹ was the origin band was provided by the DLIF spectrum shown in Fig. 7. Despite the low resolution of this scan, it is evident that a progression in the Yb-OH stretch was observed [with an average vibrational interval of 530(10) cm⁻¹] and the intensity envelope was typical of the emission from a zero-point vibrational state.

Figure 8 shows a higher-resolution scan of the origin band, where partial resolution of the rotational structure has been achieved. This band exhibits the *P*- and *R*-branch lines ex-

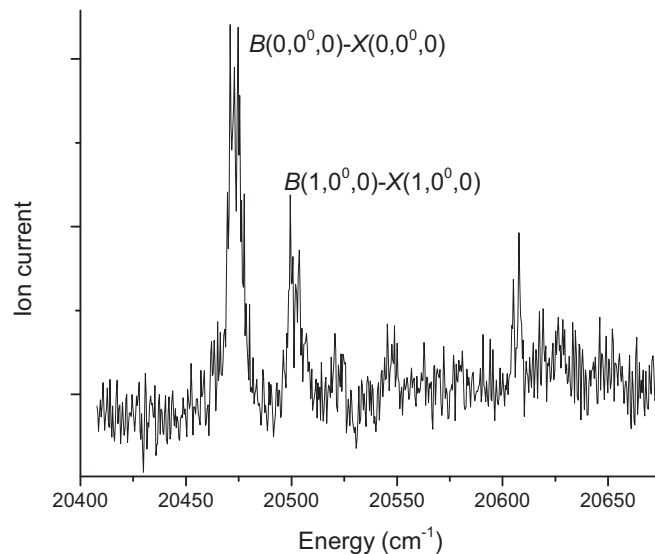


FIG. 6. Low-resolution RE2PI scan of the origin-band region of the $\tilde{B}^2\Sigma^+-\tilde{X}^2\Sigma^+$ transition of YbOH.

pected for a $^2\Sigma^+-^2\Sigma^+$ transition, but attempts to fit the structure with a simple model were not satisfactory. The downward-pointing trace in Fig. 8 is a simulation generated using the PGOPHER software package [24]. This was based on the assumption of a $^2\Sigma^+-^2\Sigma^+$ transition with the ground-state constants set to the literature values of $B'' = 0.2452$ and $\gamma'' = 0.0027$ cm⁻¹ (where γ is the spin-rotation interaction constant) [25]. The rotational temperature was set to 15 K, where rotational levels ranging from $N = 0$ to 12 can be discerned (levels up to $N = 50$ were included in the simulation, where N is the quantum number for the angular momentum excluding the spin). An approximate fit to the experimental data was achieved using the upper-state constants $T_0 = 20 473.8$, $B' = 0.254$, and $\gamma' = 0.05$ cm⁻¹. The unusually

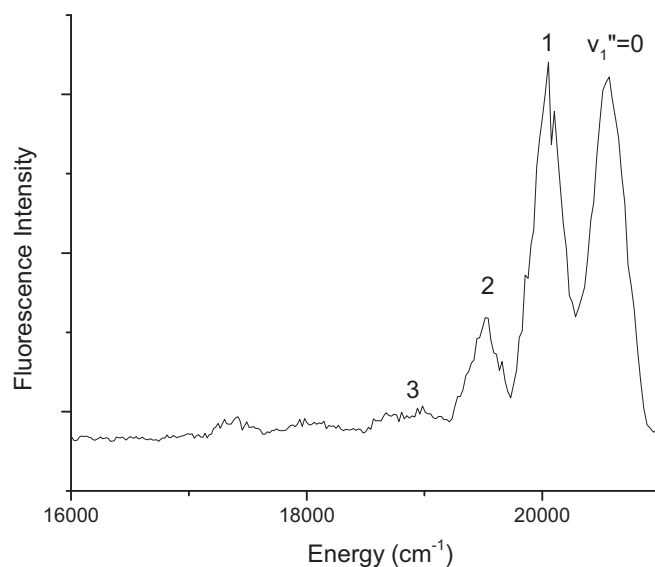


FIG. 7. DLIF spectrum obtained by exciting the $\tilde{B}^2\Sigma^+(0,0^0,0)-\tilde{X}^2\Sigma^+(0,0^0,0)$ origin transition of YbOH.

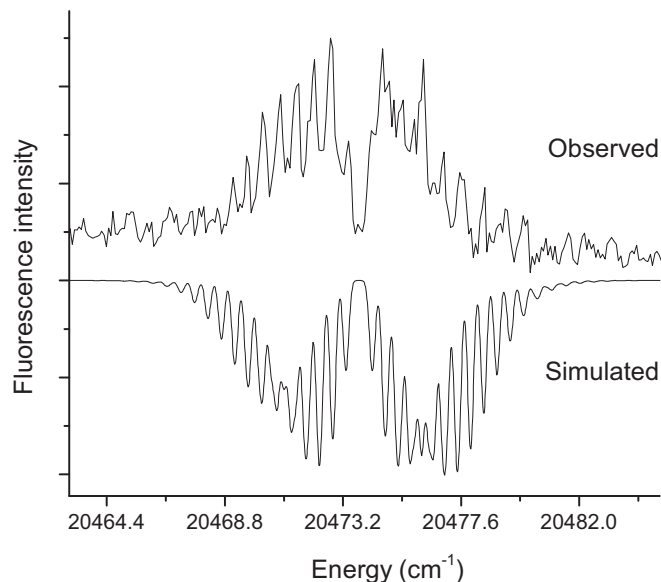


FIG. 8. Spectrum of the $\tilde{B}^2\Sigma^+(0,0^0,0) - \tilde{X}^2\Sigma^+(0,0^0,0)$ transition of YbOH showing partial resolution of the rotational structure. The downward-pointing trace is a simulation generated using the PGOPHER software. See text for details.

large spin-rotation constant and the imperfections of the fit both indicate the presence of perturbations. In this context it is of interest to note that Barrow and Chojnicki [23] were unable to fit the rotational structure of the YbF $B^2\Sigma^+ - \tilde{X}^2\Sigma^+$ origin band due to the presence of perturbations.

The fluorescence decay of YbOH $\tilde{B}^2\Sigma^+, (0,0^0,0)$ was recorded and fit to a single-exponential decay, yielding a lifetime of 31(5) ns.

D. Ionization energies of YbOH and YbOCH₃

The ionization energies of YbOH and YbOCH₃ were determined by recording PIE curves. Figures 9 and 10 show the ionization onsets. For YbOH the first laser was tuned to excite the $\tilde{A}^2\Pi_{1/2} - \tilde{X}^2\Sigma^+$ origin band at 17 323 cm⁻¹. The onset of ionization was then observed by sweeping the energy of the second photon while monitoring the production of YbOH⁺. The result, shown in Fig. 9, has an onset at 28 350(20) cm⁻¹. Adding the photon energies and correcting for the local electric-field depression of the IE we obtained a field-free value of 45 788(20) cm⁻¹ [5.6770(12) eV].

The PIE curve for YbOCH₃ is presented in Fig. 10. For this measurement the first laser was set to excite the 17 642 cm⁻¹ band. There is a small feature at 27 520 cm⁻¹ that we identified as a resonantly enhanced one-color, two photon ionization process. This was present for a scan of the second laser with the first laser blocked. Hence, we estimate that the PIE signal has an onset near 27 525 cm⁻¹, and the field-free ionization energy is 45 282(15) cm⁻¹ [5.6144(18) eV].

III. DISCUSSION

The molecules YbF, YbOH, and YbOCH₃ have similar electronic structures, with ground states that are well represented by the configuration Yb⁺(4f¹⁴, 6s¹)X⁻, where

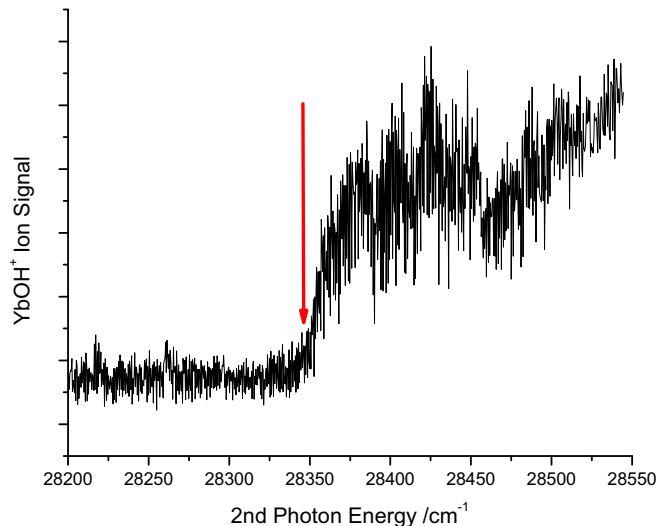


FIG. 9. Photoionization efficiency curve for YbOH. This trace was recorded with the first laser tuned to the YbOH $\tilde{A}^2\Pi_{1/2}(0,0^0,0) - \tilde{X}^2\Sigma^+(0,0^0,0)$ transition at 17 323 cm⁻¹. The arrow indicates the visually estimated onset of ionization.

X⁻ is a closed-shell anion. However, the electronic structure of the low-energy states is complicated by the presence of states arising from the Yb⁺(4f¹³, 6s²)X⁻ configuration. The interactions between the Yb⁺(4f¹⁴, 6p¹)X⁻ and Yb⁺(4f¹³, 6s²)X⁻ states result in vibronically coupled manifolds that are difficult to assign for the polyatomic molecules [7,9,10,22,25]. The brief study of the YbOD $\tilde{A}^2\Pi_{1/2} - \tilde{X}^2\Sigma^+$ bands reported here provides some new information concerning the bending vibrations.

Based upon the isotopic shifts, the previously observed band of YbOH at 17 332 cm⁻¹ [10] has been reassigned as the $\tilde{A}^2\Pi_{1/2}(0,1,0) - \mu^2\Sigma - \tilde{X}^2\Sigma^+(0,1^1,0)$ band. This transition will be particularly useful for detection of

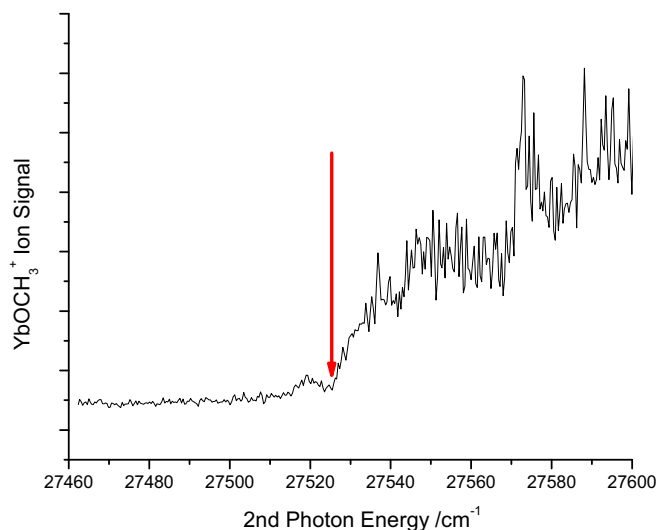


FIG. 10. Photoionization efficiency curve for YbOCH₃. This trace was recorded with the first laser tuned to the YbOCH₃ [17.64] $- \tilde{X}^2\Sigma^+(0,0^0,0)$ band at 17 642 cm⁻¹. Arrow indicates the visually estimated onset of ionization.

the eEDM-sensitive degenerate vibronic level. A band at 17339 cm^{-1} , which was previously observed in the spectrum of a high-temperature sample [22] and assigned to the $\tilde{A}^2\Pi_{1/2}(0, 1, 0)\mu^2\Sigma^+-\tilde{X}^2\Sigma^+(0, 1^1, 0)$ transition, is reassigned as the $\tilde{A}^2\Pi_{1/2}(0, 2^0, 0)-\tilde{X}^2\Sigma^+(0, 2^0, 0)$ band. Interestingly, based upon the observed YbOH–YbOD isotopic shifts none of the previously observed bands [10] could be assigned to the $\tilde{A}^2\Pi_{1/2}(0, 1, 0)\mu^2\Sigma^+-\tilde{X}^2\Sigma^+(0, 0^0, 0)$ transition. Although nominally symmetry forbidden, linear vibronic coupling and spin-orbit coupling between the $\tilde{A}^2\Pi$ and $\tilde{B}^2\Sigma^+$ states can mix the $\tilde{A}^2\Pi_{1/2}(0, 1, 0)\mu^2\Sigma^+$ and $\tilde{A}^2\Pi_{1/2}(0, 0^0, 0)$ states which, as demonstrated in the case of SrOH [26], can make the $\tilde{A}^2\Pi_{1/2}(0, 1, 0)\mu^2\Sigma^+-\tilde{X}^2\Sigma^+(0, 0^0, 0)$ transition readily observable.

The similarity of YbF and YbOH was used to discover the $\tilde{B}^2\Sigma^+-\tilde{X}^2\Sigma^+$ transition of YbOH. The origin band at 20473.8 cm^{-1} was just 600 cm^{-1} below the corresponding transition of YbF [23]. In keeping with the notion that the Yb $6s$ and $6p$ orbitals are both slightly antibonding, the rotational structure of the $\tilde{B}-\tilde{X}$ origin band indicated only a small change in the equilibrium Yb–OH distance on electronic excitation. The short radiative lifetime of the \tilde{B} state and the fact that only $\tilde{B}-\tilde{X}$ bands were present in the DLIF spectrum indicates that the $\tilde{B}-\tilde{X}$ transition is fully electric-dipole allowed.

A recent study [11] of YbOH included a high-level computational study of the $\tilde{X}^2\Sigma^+$, $\tilde{A}^2\Pi_{1/2}$, and $\tilde{B}^2\Sigma^+$ states.

Potential-energy surfaces were obtained, and used to predict the energies of vibrational eigenstates using the discrete variable representation method. For the $\tilde{A}^2\Pi_{1/2}$ state, Zhang *et al.* [11] reported a Yb–OH vibrational interval of 562 cm^{-1} , which is 11 cm^{-1} lower than the measured value of 573 cm^{-1} . The first bending vibrational interval was predicted to be 333 cm^{-1} , in good agreement with the experimental value of 338 cm^{-1} obtained from our revised assignment of the band at 17332 cm^{-1} .

Although it was not reported in Ref. [11], the separation between the $\tilde{B}^2\Sigma^+(0, 0^0, 0)$ and $\tilde{A}^2\Pi_{1/2}(0, 0^0, 0)$ states was calculated to be 2935 cm^{-1} [14], which, when combined with the experimental origin for the $\tilde{A}^2\Pi_{1/2}(0, 0^0, 0)-\tilde{X}^2\Sigma^+(0, 0^0, 0)$ band ($=17323\text{ cm}^{-1}$) gives a predicted term energy for the $\tilde{B}^2\Sigma^+(0, 0^0, 0)$ state of 20258 cm^{-1} , which is 216 cm^{-1} below the measured value. The computed first Yb–OH vibrational interval for the \tilde{B} state was 559 cm^{-1} , in agreement with the measured value of 560 cm^{-1} .

The $\tilde{B}^2\Sigma^+$ state is likely to be responsible for the observed Λ doubling in the $\tilde{A}^2\Pi_{1/2}(0, 0^0, 0)T_0 = 17323\text{ cm}^{-1}$ state. The effective Λ -doubling constant, $p + 2q$, for the $\tilde{A}^2\Pi_{1/2}(0, 0^0, 0)$ state, which will be dominated by p , was determined [27] to be $= -0.43807\text{ cm}^{-1}$. The p parameter is given by the second-order perturbation expression [28]:

$$p^{\Pi}(^2\Sigma^+) = 2 \sum_{^2\Sigma^+, v'} \frac{\langle ^2\Pi, v | \sum_i a_i l_i^+ s_i^- | ^2\Sigma^+, v' \rangle \langle ^2\Sigma^+, v' | \frac{\hbar^2}{2I_{aa}} \sum_i l_i^- | ^2\Pi, v \rangle}{E_{\Pi, v} - E_{\Sigma, v'}}, \quad (1)$$

where $^2\Sigma^-$ states have been excluded from the summation and I_{aa} is the component of the moment of inertia tensor. If we assume that the $\tilde{A}^2\Pi_{1/2}$ and $\tilde{B}^2\Sigma^+$ states arise from π^1 and σ^1 configurations and form a p complex, then

$$p^{\Pi}(^2\Sigma^+) \approx 4A_{\text{SO}}B \sum_{v'} \frac{\langle v | v' \rangle}{E_{\Pi, v} - E_{\Sigma, v'}}, \quad (2)$$

where B is the average value of the rotational constant of the $\tilde{A}^2\Pi_{1/2}$ and $\tilde{B}^2\Sigma^+$ states ($\sim 0.253\text{ cm}^{-1}$) [22]. Taking $E_{\Sigma^+, v'}$ for the $\tilde{B}(0, 0^0, 0)$ state as 20473 cm^{-1} and assuming identical potential-energy curves for the $\tilde{B}^2\Sigma^+$ and $\tilde{A}^2\Pi$ states in the region of the equilibrium geometry (i.e., $\langle v_i | v_j \rangle = \delta_{ij}$), Eq. (2) gives $p^{\text{calc}} = -0.433\text{ cm}^{-1}$, which is in good agreement with the observed value of -0.43807 cm^{-1} .

Mengesha *et al.* [10] identified the lowest-energy component ($\Omega = 1/2$) of the $\text{Yb}^+(4f^{13}(^2F_{5/2})6s^2)\text{OH}^-$ electronic configuration at an energy of 17730 cm^{-1} . States arising from the $\text{Yb}^+(4f^{13}(^2F_{7/2})6s^2)\text{OH}^-$ configuration were not observed in the present study, but the energy of the $\Omega = 1/2$ component can be estimated using the spin-orbit interval for the free-atomic $\text{Yb}(4f^{13}6s^2)^+$ ion. The data for $\text{Yb}^+(4f^{13}(^2F_j)6s^2)\text{F}^-$ show that the energy difference between the $\Omega = 1/2$ components of the $j = 5/2$ and $j = 7/2$ states is 10099 cm^{-1} , just 50 cm^{-1} lower than the corresponding interval of the free-atomic ion (10149 cm^{-1}) [29]. If it is

assumed that the same spin-orbit interval would be valid for YbOH, the $\text{Yb}^+(4f^{13}(^2F_{7/2})6s^2)\text{F}^-$, $\Omega = 1/2$ would be near 7630 cm^{-1} .

We have reported the IE of YbF previously [48703(5) cm^{-1}] [13] and the present study provides IE values of $45788(10)$ and $45283(10)\text{ cm}^{-1}$ for YbOH and YbOCH_3 , respectively. We briefly examined the ability of commonly used electronic structure models to predict the IE of YbOH. These calculations employed a 28-electron relativistic effective-core potential for Yb, which was combined with a valence basis of quadruple-zeta quality (Stuttgart RSC Seg + ECP28MB). Augmented valence quadruple-zeta basis sets were used for O and H. The calculations were carried out using the MOLPRO suite of computer codes [30], and all methods converged to linear equilibrium structures for both the ion and the neutral. Density functional theory - Becke, 3-parameter, Lee-Yang-Parr (DFT-B3LYP) calculations yielded bond lengths of $R_{\text{YbO}} = 2.043(1.967)$ and $R_{\text{OH}} = 0.937(0.956)\text{ \AA}$, where the numbers in parentheses are for the cation. The adiabatic IE was predicted to be 45476 cm^{-1} , in good agreement with the measured value. Modest-level coupled-cluster treatments were less accurate. Coupled cluster singles and doubles (CCSD) calculations gave equilibrium bond lengths of $R_{\text{YbO}} = 2.041(1.964)$ and $R_{\text{OH}} = 0.949(0.951)\text{ \AA}$, and an adiabatic IE of 43950 cm^{-1} . A single-point Coupled cluster singles, doubles and perturbative triples (CCSD(T))

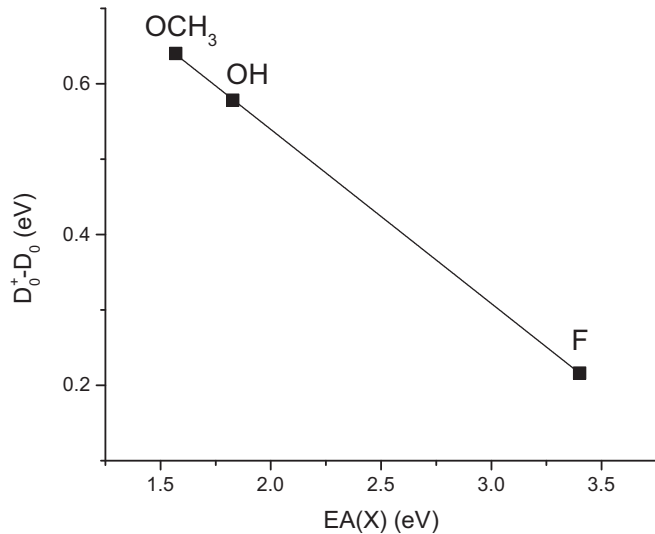


FIG. 11. Plot of the bond-energy difference for the ion and neutral YbX molecule vs the electron affinity of X.

calculation, carried out at the CCSD equilibrium geometry for the neutral molecule, returned a vertical IE of $44\,492\text{ cm}^{-1}$.

The energy difference between the IE of YbX and that of atomic Yb defines the difference between the bond-dissociation energies (BDE) of the cationic and neutral molecules, such that

$$\text{IE}(\text{Yb}) - \text{IE}(\text{YbX}) = D_0^+ - D_0. \quad (3)$$

The molecular IE's are all smaller than $\text{IE}(\text{Yb})$ (6.2542 eV , $50\,444\text{ cm}^{-1}$) [31], indicating that the molecular cations are all more deeply bound than the neutrals. This can be understood in terms of the elimination of the electrostatic repulsion between the X^- ligand and $\text{Yb } 6s^1$. As these molecules have a strong ionic component in their bonding, it is of interest to examine the dependence of the $D_0^+ - D_0$ energy differences on the electron affinities (EA) of the ligand X. Using literature values of $\text{EA}(\text{F}) = 3.401$ [32], $\text{EA}(\text{OH}) = 1.828$ [33], and $\text{EA}(\text{OCH}_3) = 1.569\text{ eV}$ [34], we obtained a surprisingly good linear relationship as shown in Fig. 11. The negative slope of this plot suggests that it is the change in the neutral-molecule BDE that is most important.

Data concerning the BDE's of YbOH^+ and YbF^+ present a puzzle that was recently discussed in the work of Parker *et al.* [16]. These investigators observed the reaction $\text{Yb}^+ + \text{H}_2\text{O} \rightarrow \text{YbOH}^+ + \text{H}$ in a quadrupole ion-trap mass spectrometer, where the slow but spontaneous process implied a lower bound for the YbOH^+ BDE of $\geq 5.17\text{ eV}$ [16]. The authors noted that, "This limit is significantly higher than previously reported for YbOH^+ and is unexpectedly similar to the BDE for $\text{Yb}^+ - \text{F}$." The $\text{Yb}^+ + \text{D}_2\text{O}$ reaction had also been seen in a selected-ion flow-tube experiment [17]. However, using a Fourier transform ion cyclotron resonance mass spectrometer, Carretas *et al.* [18] did not observe reactions of Yb^+ with methanol or ethanol, where the OH group is less strongly bound than in H_2O . As a possible resolution of

this discrepancy, Parker *et al.* [16] noted that "the inefficient hydrolysis reactions observed here in a quadrupole ion trap mass spectrometer may actually be endothermic."

As there is considerable uncertainty in the BDE's of YbX and YbX^+ , our measurements of the IE's cannot resolve the conflicts. However, our results can be used to improve BDE estimates that have been obtained using Eq. (3). For example, the previously accepted IE's for YbOH [$6.04(5)\text{ eV}$] [35] and YbF [$5.90(7)\text{ eV}$] [36] were in error by $+0.36$ and -0.14 eV , respectively. Belyaev *et al.* [37] obtained an estimate of $D_0(\text{YbOH}) = 3.91(8)\text{ eV}$ from spectroscopic measurements. When combined with the earlier estimation of the IE for YbOH [35], this yielded a BDE for YbOH^+ of $4.14(10)\text{ eV}$. Correcting the IE increases the YbOH^+ BDE to $4.49(10)\text{ eV}$. This value is still considerably lower than the upper bound derived from the $\text{Yb}^+ + \text{H}_2\text{O}$ reaction, which may indicate that the neutral-molecule BDE derived from the spectroscopic data is underestimated.

IV. SUMMARY

The $\tilde{A}^2\Pi_{1/2} - \tilde{X}^2\Sigma^+$ transition of YbOH/D has been examined using RE2PI spectroscopy with mass-resolved ion detection. The observed isotopic shifts of the present study have provided a reassignment of weak bands in the previously reported visible LIF spectrum [10]. Most notably, bands associated with the degenerate bending mode of the ground electronic state, which is of particular interest for investigations parity-violating effects, have been unambiguously identified. Previously it was noted that the vibronic structure of the $\tilde{A}^2\Pi_{1/2}$ state was perturbed by mixing with nearby states arising from the $\text{Yb}^+(4f^{13} 6s^2)\text{OH}^-$ electronic configuration. These interactions complicate the isotope shift behavior, such that only a qualitative estimate for the involvement of the bending motion in a given vibronic state could be deduced. The $\tilde{B}^2\Sigma^+ - \tilde{X}^2\Sigma^+$ transition for YbOH was observed, providing the term energy, $\Delta G_{1/2}$ vibrational interval and radiative lifetime of the \tilde{B} state.

The possibility that YbOH and YbOCH_3 may be laser cooled has motivated several recent spectroscopic studies of these molecules. As both can be produced by the reaction of Yb vapor with CH_3OH , we have used RE2PI to identify band overlaps at $17\,641$ and $17\,683\text{ cm}^{-1}$ for the low-energy range of the $\tilde{A} - \tilde{X}$ transitions.

Ionization energies for YbOH and YbOCH_3 were measured using a two-color threshold photoionization technique. The IE for YbOH was found to be 0.36 eV below the accepted literature value, while the IE for YbOCH_3 had not been reported previously. The revised IE for YbOH contributes to the resolution of conflicting data for the bond-dissociation energies of YbOH and YbOH^+ .

ACKNOWLEDGMENT

This material is based upon work supported by the U.S. Department of Energy, Office of Science, Office of Basic Energy Sciences, Heavy Element Chemistry program under Award No. DE-FG02-01ER15153. T. C. Steimle and A. Le supported by Heising-Simons Foundation (Grant No. 2018-0681).

- [1] J. Lim, J. R. Almond, M. A. Trigatzis, J. A. Devlin, N. J. Fitch, B. E. Sauer, M. R. Tarbutt, and E. A. Hinds, *Phys. Rev. Lett.* **120**, 123201 (2018).
- [2] X. Alauze, J. Lim, M. A. Trigatzis, S. Swarbrick, N. J. Fitch, B. E. Sauer, and M. R. Tarbutt, *Quantum Sci. Technol.* **6**, 044005 (2021).
- [3] B. L. Augenbraun, Z. D. Lasner, A. Frenett, H. Sawaoka, C. Miller, T. C. Steimle, and J. M. Doyle, *New J. Phys.* **22**, 022003 (2020).
- [4] N. B. Vilas, C. Hallas, L. Anderegg, P. Robichaud, A. Winnicki, D. Mitra, and J. M. Doyle, *Nature (London)* **606**, 70 (2022).
- [5] N. R. Hutzler, *Quantum Sci. Technol.* **5**, 044011 (2020).
- [6] I. Kozryyev and N. R. Hutzler, *Phys. Rev. Lett.* **119**, 133002 (2017).
- [7] B. I. Augenbraun, Z. D. Lasner, A. Frenett, H. Sawaoka, A. T. Le, J. M. Doyle, and T. C. Steimle, *Phys. Rev. A* **103**, 022814 (2021).
- [8] G.-Z. Zhu *et al.*, *Nat. Chem.* **14**, 995 (2022).
- [9] N. H. Pilgram, A. Jadbabaie, Y. Zeng, N. R. Hutzler, and T. C. Steimle, *J. Chem. Phys.* **154**, 244309 (2021).
- [10] E. T. Mengesha, A. T. Le, T. C. Steimle, L. Cheng, C. Zhang, B. L. Augenbraun, Z. Lasner, and J. Doyle, *J. Phys. Chem. A* **124**, 3135 (2020).
- [11] C. Zhang, B. L. Augenbraun, Z. D. Lasner, N. B. Vilas, J. M. Doyle, and L. Cheng, *J. Chem. Phys.* **155**, 091101 (2021).
- [12] C. Zhang, C. Zhang, L. Cheng, T. C. Steimle, and M. R. Tarbutt, *J. Mol. Spectrosc.* **386**, 111625 (2022).
- [13] T. D. Persinger, J. Han, A. T. Le, T. C. Steimle, and M. C. Heaven, *Phys. Rev. A* **106**, 062804 (2022).
- [14] L. Cheng and C. Zhang (unpublished).
- [15] M. C. Heaven, *Phys. Chem. Chem. Phys.* **8**, 4497 (2006).
- [16] M. L. Parker, J. Jian, and J. K. Gibson, *Phys. Chem. Chem. Phys.* **23**, 11314 (2021).
- [17] P. Cheng, G. K. Koyanagi, and D. K. Bohme, *ChemPhysChem* **7**, 1813 (2006).
- [18] J. M. Carretas, J. Marcalo, and A. Pires de Matos, *Int. J. Mass Spectrom.* **234**, 51 (2004).
- [19] M. A. Duncan, *Rev. Sci. Instrum.* **83**, 041101/1 (2012).
- [20] T. D. Persinger, J. Han, and M. C. Heaven, *J. Phys. Chem. A* **125**, 3653 (2021).
- [21] G. Herzberg, *Electronic Spectra and Electronic Structure of Polyatomic Molecules (Molecular Spectra and Molecular Structure, Vol. III)* (Van Nostrand Reinhold Company, New York, 1966).
- [22] T. C. Melville and J. A. Coxon, *J. Chem. Phys.* **115**, 6974 (2001).
- [23] R. F. Barrow and A. H. Chojnicki, *J. Chem. Soc., Faraday Trans. 2* **71**, 728 (1975).
- [24] C. M. Western, *J. Quant. Spectrosc. Radiat. Transfer* **186**, 221 (2017).
- [25] J. A. Coxon and C. Linton, *J. Mol. Spectrosc.* **367**, 111242 (2020).
- [26] P. I. Presunka and J. A. Coxon, *J. Chem. Phys.* **101**, 201 (1994).
- [27] T. C. Steimle, C. Linton, E. T. Mengesha, X. Bai, and A. T. Le, *Phys. Rev. A* **100**, 052509 (2019).
- [28] R. W. Field, *Spectra and Dynamics of Small Molecules: Alexander von Humboldt Lectures*, Lectures Notes in Physics, Vol. 900 (Springer, Switzerland, 2015).
- [29] A. Kramida, Yu. Ralchenko, J. Reader, and NIST ASD Team (2022). NIST Atomic Spectra Database (version 5.10), 2023, available at <https://physics.nist.gov/asd>, National Institute of Standards and Technology, Gaithersburg, MD, doi: <https://doi.org/10.18434/T4W30F>.
- [30] H.-J. Werner, P. J. Knowles, G. Knizia, F. R. Manby, and M. Schuetz, *Wiley Interdiscip. Rev., Comput. Mol. Sci.* **2**, 242 (2012).
- [31] M. Aymar, A. Debarre, and O. Robaux, *J. Phys. B* **13**, 1089 (1980).
- [32] C. Blondel, C. Delsart, and F. Goldfarb, *J. Phys. B* **34**, L281 (2001).
- [33] F. Goldfarb, C. Drag, W. Chaibi, S. Kröger, C. Blondel, and C. Delsart, *J. Chem. Phys.* **122**, 014308 (2004).
- [34] M. J. Nee, A. Osterwalder, J. Zhou, and D. M. Neumark, *J. Chem. Phys.* **125**, 014306 (2006).
- [35] V. N. Belyaev, N. L. Lebedeva, and K. S. Krasnov, *Zh. Fiz. Khim.* **70**, 1429 (1996).
- [36] A. A. Kitaev, I. S. Gotkis, P. G. Val'kov, and K. S. Krasnov, *Izv. Vyssh. Uchebn. Zaved., Khim. Khim. Tekhnol.* **31**, 56 (1988).
- [37] V. N. Belyaev and N. L. Lebedeva, *Zh. Fiz. Khim.* **72**, 2176 (1998).